Heat Transfer in a Bundle Cooled with Supercritical Freon-12

Wargha Peiman, Ashley Milner, Caleb Pascoe, Hemal Patel, Graham Richards, and Igor Pioro

University of Ontario Institute of Technology
Faculty of Energy Systems and Nuclear Science
2000 Simcoe Street North, Oshawa, Ontario, L1H 7K4, Canada
E-mail: wargha.peiman@mycampus.uoit.ca and igor.pioro@uoit.ca

Abstract

This paper focuses on analyzing experimental data on Freon-12 at a supercritical pressure of 4.65 MPa. Experiments were conducted at the Institute of Physics and Power Engineering in Russia. The test section consisted of a pressure tube, ceramic inserts, a hexagonal flow tube and a vertical 7-element bundle installed inside the flow tube. The seven elements of the bundle were made of stainless steel and had an outer diameter of 9.5 mm and a heated length of one meter. Bulk-fluid temperature of the coolant at the inlet and the outlet of the test section and the temperature profile of the central heated element were recorded using thermocouples. For comparison, bulk-fluid, and sheath temperature profiles were calculated using various correlations and results were compared with the experimental values.

NOMENCLATURE

A	cross-sectional area, m^2
A_{fl}	flow area, m^2
C_p	specific heat at constant pressure, J/kg K
$\bar{C}_p$	averaged specific heat, $(\frac{H_w - H_b}{T_w - T_b})$, J/kg K
D	diameter, m
D_{hy}	hydraulic diameter, m
G	mass flux, (m/A_{fl}), kg/m^2 s
g	gravitational acceleration, m/s^2
h	heat transfer coefficient, W/m K
h	enthalpy, J/kg
k	thermal conductivity, W/m K
L_c	characteristic length, m
m	mass flow rate, kg/s
P	pressure, Pa
Q	heat transfer rate, W

q	heat flux, W/m^2
T	temperature,

Greek symbols

α	thermal diffusivity, ($k/\rho\ C_p$), m^2/s
β	volumetric thermal expansion coefficient, ($1/T$), 1/K
σ	Stefan–Boltzmann constant, W/m^2 K^4
ν	kinematic viscosity, m^2/s
μ	dynamic viscosity, kg/m s
ρ	density, kg/m^3

Non-dimensional numbers

$\mathbf{Nu}_D$	Nusselt number, $\mathbf{Nu}_D = h \cdot D/k$
$\mathbf{Pr}$	Prandtl Number, $\overline{\mathbf{Pr}} = \mu \cdot C_p/k$
$\overline{\mathbf{Pr}}$	averaged Prandtl Number, $\overline{\mathbf{Pr}} = \mu \cdot \bar{C}_p/k$
$\mathbf{Ra}_c$	Rayleigh number, $\mathbf{Ra}_c = \frac{g\beta(T_i - T_o)L_c^3}{\nu\alpha}$
$\mathbf{Re}_D$	Reynolds number, $\mathbf{Re}_{\boldsymbol{D}} = \boldsymbol{G} \cdot \frac{\boldsymbol{D_{hy}}}{\boldsymbol{\mu}}$

Subscripts

b	properties calculated at bulk fluid temperature
cond	conduction
conv	convection
i	inner
o	outer
pc	pseudocritical point
w	properties calculated at wall temperature

Abbreviations

DHT	Deteriorated Heat Transfer
GIF	Generation IV International Forum
HTC	Heat Transfer Coefficient
IHT	Improved Heat Transfer
NIST	National Institute of Standards and Technology (USA)
NPP	Nuclear Power Plant
SCWR	SuperCritical Water-cooled Reactor

1. Introduction

The need to meet the current and future demands of electricity and to address environmental challenges such as global warming has opened a new vista for international collaboration to carry out the research and development required to develop the next generation of nuclear reactors categorized as Generation IV system. Six systems have been selected to be studied under the Generation IV International Forum (GIF), one of which is a SuperCritical Water-cooled Reactor (SCWR) option. The ultimate goal of Generation IV technologies is to increase the thermal efficiency of Nuclear Power Plants (NPPs) above those of the current conventional NPPs with thermal efficiencies between 30 and 36%.

Currently, many countries worldwide are developing SCWR concepts. The development of SCW NPPs is gaining momentum. However, the genesis of that idea occurred at the end of the 1950s through the 1970s during which the possibility of SCW NPPs was investigated and some initial designs were developed [1]. Some of the advantages of the SCW NPPs over conventional NPPs include higher thermal efficiency (approximately 45 − 50%), lower capital costs per kWh of electricity, and the possibility for co-generation of hydrogen through thermo-chemical cycles.

The development of SCWRs requires an intensive study of convective heat transfer at supercritical pressures. Heat transfer at a supercritical pressure is different from that of at a subcritical pressure because thermophysical properties of the coolant undergo significant variations as the temperature of the coolant passes through the pseudocritical point. Therefore, the Nusselt number and other non-dimensional parameters developed at a subcritical pressure heat transfer based on bulk-fluid temperature cannot be used [2]. Additionally, the wall temperature plays an important role at supercritical conditions.

The properties of a coolant at a supercritical pressure at the wall temperature significantly differ from those at the bulk-fluid temperature. Therefore, the wall temperature must be reflected in a correlation, which is used to study the heat transfer [2]. A fluid does not undergo phase change at a supercritical pressure. However, a low-density fluid separates the wall from the high-density fluid at high heat fluxes and results in a reduction in the convective Heat Transfer Coefficient (HTC) and a consequent increase in the wall temperature. This phenomenon is called Deteriorated Heat Transfer (DHT).

2. Modelling Fluids

The development of the SCWR concept requires experimental data on heat transfer to water at supercritical conditions. SCWRs operate above the critical point of water (a temperature of 374℃ and a pressure of 22.1 MPa). It is a common practice to use other fluids, which have lower critical parameters compared to those of water. This allows experiments to be performed at lower temperatures and pressures, which in turn reduces experimental costs and allows for a wider experimental range [3]. Carbon dioxide and Freon-12[1] are the most common modeling fluids at supercritical pressures.

Operating conditions of a modeling fluid must be scaled to those of supercritical water in order to provide a degree of comparison between the two fluids. Therefore, scaling parameters are required to convert a modeling fluid's operating conditions such as pressure, bulk-fluid temperature, mass flux, and heat flux to equivalent values of supercritical water. Reference [1] offers scaling parameters for fluid-to-fluid modeling at supercritical conditions. These parameters are listed in Table 1 [1].

Table 1: Scaling Parameters for Fluid-to-Fluid Modeling at Supercritical Conditions [1].

Parameter	**Equation**
Pressure	$(P/P_{cr})_A = (P/P_{cr})_B$
Bulk-fluid Temperature (K)	$(T_b/T_{cr})_A = (T_b/T_{cr})_B$
Heat Flux	$(qD/k_b \cdot T_b)_A = (qD/k_b \cdot T_b)_B$
Mass Flux	$(G \cdot D/\mu_b)_A = (G \cdot D/\mu_b)_B$
Heat Transfer Coefficient	$\mathbf{Nu}_A = \mathbf{Nu}_B$

R-134a has been chosen as a replacement refrigerant for R-12. Firstly, R-134a is regarded as one of the safest refrigerants in terms of toxicity. In other words, R-134a does not pose cancer or birth defect hazards. Secondly, unlike R-12, R-134a is not flammable at room temperatures and atmospheric pressures. Moreover, R-134a is not corrosive on materials such as steel, aluminium, or copper. Thirdly, in terms of depletion of ozone layer, R-134a has no negative impact on the ozone layer; however, the ozone depletion ranking for R-12 is one compared to zero for R-134a [4]. Finally, thermophysical properties of R-134a and R-12 slightly differ. For instance, the boiling point of R-134a is 247.0 K and that of R-12 is 243.3 K at atmospheric pressure [5].

3. Thermophysical Properties

Heat transfer at supercritical conditions is characterized by changes in thermophysical properties of the fluid, specifically at a pseudocritical point at which the thermophysical properties undergo significant changes affecting the heat transfer capabilities of the fluid. The pseudocritical point is defined as a point at a pressure above the critical pressure and at a temperature corresponding to the maximum value of specific heat for this particular pressure [1]. Figures 1 and 2 show general trends of the specific heat of water and Freon-12. The properties were obtained through NIST REFPROP software [5]. Additionally, Table 2 provides the critical point and pseudocritical temperatures of water and Freon-12 at 25 MPa and 4.65 MPa, respectively.

[1] Currently, Freon-12 is replaced with Freon-134a

Table 2: Critical and Pseudocritical Points of Water and Freon-12.

Parameter	Light Water		Freon-12	
	P, MPa	*T*, ℃	*P*, MPa	*T*, ℃
Critical Point	22.06	373.9	4.14	112.0
Pseudocritical Point	25.00	384.9	4.65	118.7

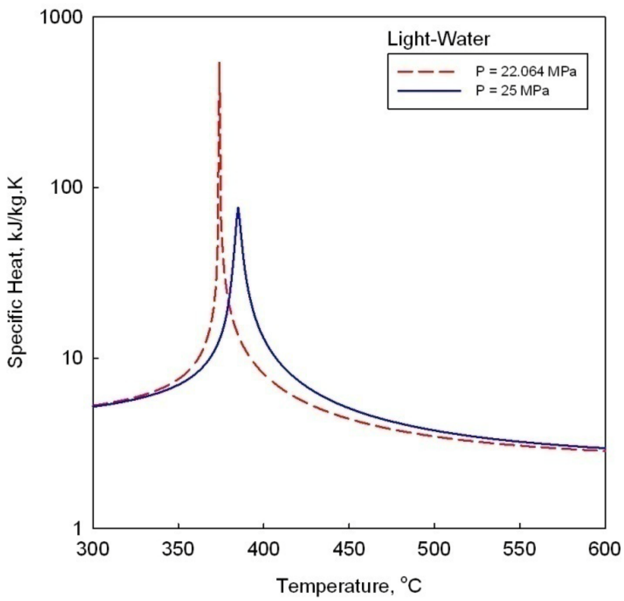

Figure 1: Specific Heat of Water as a Function of Temperature.

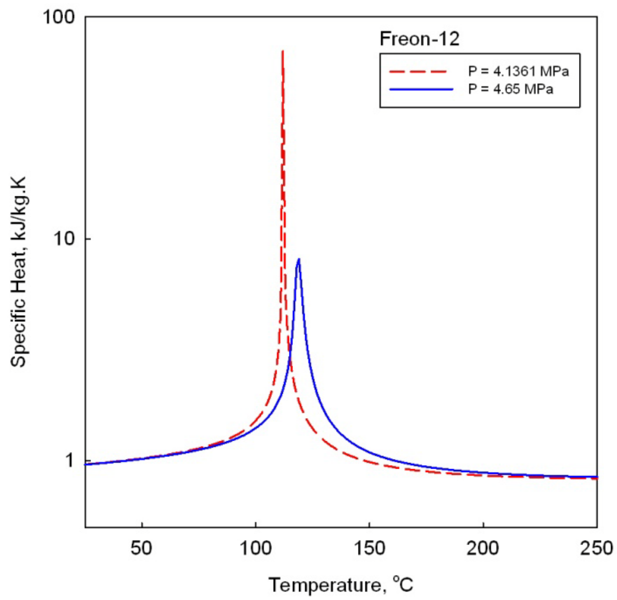

Figure 2: Specific Heat of Freon-12 as a Function of Temperature.

4. Review of Existing Correlations

Many studies have been conducted on water, CO_2, and Freon-12 at supercritical conditions within a wide range of parameters [1, 2]. As a result, a number of correlations have been developed for calculating the Nusselt number. For the purpose of this study, several well-known correlations were selected and shown as Eqs. (1 – 5).

Dittus-Boelter[2] (1930) : $\mathbf{Nu}_{\mathrm{D}} = 0.023\mathbf{Re}_D^{0.8}\mathbf{Pr}^n$ (1)

Bishop et al. (1964) : $\mathbf{Nu}_x = 0.0069\ \mathbf{Re}_x^{0.9}\ \overline{\mathbf{Pr}}_x^{0.66}\ (\frac{\rho_w}{\rho_b})_x^{0.43}\ (1 + 2.4\frac{D}{x})$ (2)

[2] It has become common practice to refer to Eq. 1 as the Dittus-Boelter correlation, the original Dittus-Boelter correlations are as follows[7]:
$\mathbf{Nu}_{\mathrm{D}} = 0.0243\ \mathbf{Re}_D^{0.8}\mathbf{Pr}^{0.4}$ (Heating)
$\mathbf{Nu}_{\mathrm{D}} = 0.0265\ \mathbf{Re}_D^{0.8}\mathbf{Pr}^{0.3}$ (Cooling)

Swenson et al. (1965): $\mathbf{Nu}_w = 0.00459\ \mathbf{Re}_w^{0.923}\ \mathbf{Pr}_w^{0.613} \left(\frac{\rho_w}{\rho_b}\right)^{0.231}$ (3)

Gorban et al. (1990): $\mathbf{Nu}_b = 0.0094\mathbf{Re}_b^{0.86}\mathbf{Pr}_b^{-0.15}$ (4)

Mokry et al. (2009): $\mathbf{Nu}_x = 0.0061\ \mathbf{Re}_x^{0.904}\ \overline{\mathbf{Pr}}_x^{0.684}\ (\frac{\rho_w}{\rho_b})_x^{0.564}$ (5)

The value of the exponent n in the Dittus-Boelter correlations is 0.4 for heating or 0.3 for cooling [7].

5. Experiments

In this paper, three experiments are presented, which were provided by Ref. [8]. Freon-12 was used as the coolant in all three experiments, which were performed at a common supercritical pressure of 4.65 MPa. In Experiment 1, the temperature of the coolant was subcritical. Experiment 2 was conducted with the temperature of the coolant changing from a subcritical to a supercritical temperature and the sheath temperature was above the pseudocritical temperature. In Experiment 3, the coolant and sheath temperatures were above the pseudocritical temperature. The results of these experiments are shown in Section 5.3.

5.1 Experimental Setup

Figures 3 and 4 show a 3-D view of the experimental test section and a schematic drawing and a cross-sectional view it, respectively [8]. The test section consisted of a hexagonal flow tube covered with ceramic rings and pressure tube with a total heated length of 1000 mm. The pressure tube was a circular pipe with an outer diameter of 40 mm and a thickness of 4 mm. The area between the hexagonal tube and the housing was filled with ceramic bushings.

There were seven circular elements of 9.5 × 0.6 mm, which were used as the model of the fuel elements. These stainless steel elements were heated with an electric current supplied through copper terminals, which were soldered to the upper ends of the elements. The surface temperature of the central element along the heated length of the channel was measured with two sliding thermal probes, which consisted of three thermo couples separated circumferentially at 120°. These three thermo couples are indicated with TC1, TC2, and TC3 in Fig. 3 [8].

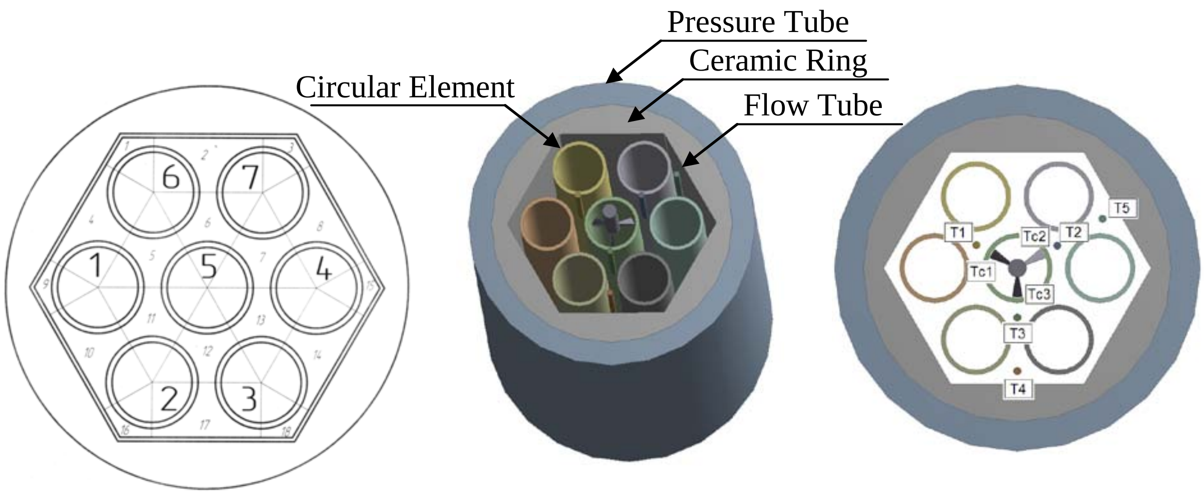

Figure 3: Cross-Sectional and 3-D View of Hexagonal Channel [8].

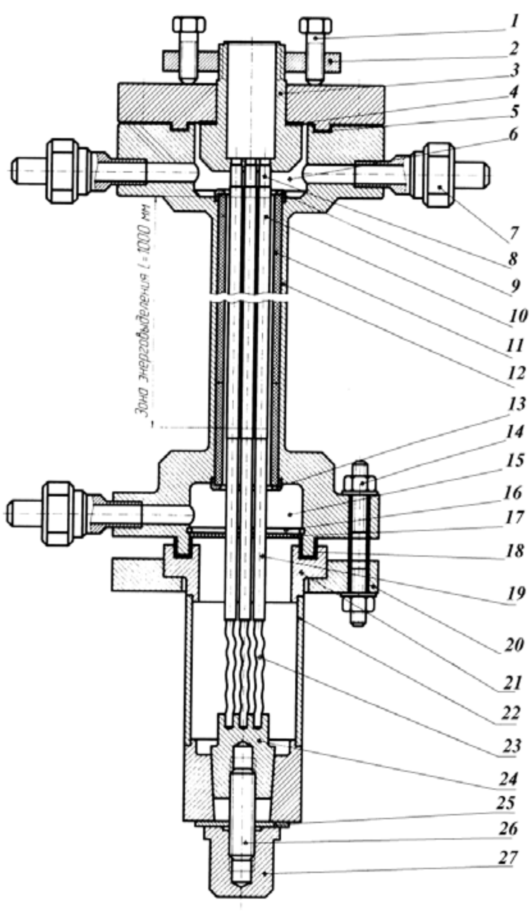

1 – holding-down bolts
2 – holding-down plate
3 – upper current terminal
4 – copper gasket
5, 18 – insulators
6 – upper chamber
7 – union
8 – copper-tube insert
9, 13 – clamp rings
10 – heated circular elements
11 – ceramic rings
12 – Pressure tube
14 – pin
15 – lower chamber
16 – check ring
17 – Teflon spacer
19 – copper rods
20 – lower flange
21 – adapter
22 – can
23 – flexible current leads
24 – cone
25 – gasket
26 – pin
27 – nut

Figure 4: Schematic View of Test Section [8].

5.2 Procedure of Experiments

Experiments were conducted after all necessary operating parameters such as pressure, temperature, and flow rate were reached and stabilized. The surface temperature of the circular element was measured using sliding thermal probes. In order to ensure the authenticity of the measurements, the temperature of the coolant was measured at the upstream and downstream chambers. Additionally, the pressure of the coolant at the inlet and the outlet of the test section were measured with strain-gauge converters. Table 3 summarizes the associated errors of various measuring devices [8]

Table 3: Experimental Errors [8].

Sensor	Error
Thermocouple	± 0.3 – 0.5 ℃
Pressure Gauge	± 0.5-1 %
Flow Meter	± 0.11 %
Power Sensor	± 2.0 %

5.3 Results of Experiments

Figure 5 shows the measured sheath temperature of the central element and the calculated temperature profile of the coolant corresponding to Experiment 1. As shown in Fig. 5, the maximum sheath temperature was below the pseudocritical temperature of the coolant. The sheath temperature increased gradually along the heated length of the channel. Additionally, no DHT regime was observed.

Figure 6 shows the distribution of the sheath temperature related to Experiment 2. A region of DHT was observed towards the inlet of the test section as indicated by the green oval. Additionally, the temperature of the sheath increased suddenly towards the outlet of the channel mostly because the temperature of the coolant approached the pseudocritical temperature. The density of the coolant decreased as its temperature approached the pseudocritical temperature (e.g., the density dropped to one-half of its value at the inlet). As a result, a low-density coolant separated the sheath from the high-density coolant. Since a low-density coolant results in a lower HTC compared to a higher density coolant, the temperature of the sheath increased.

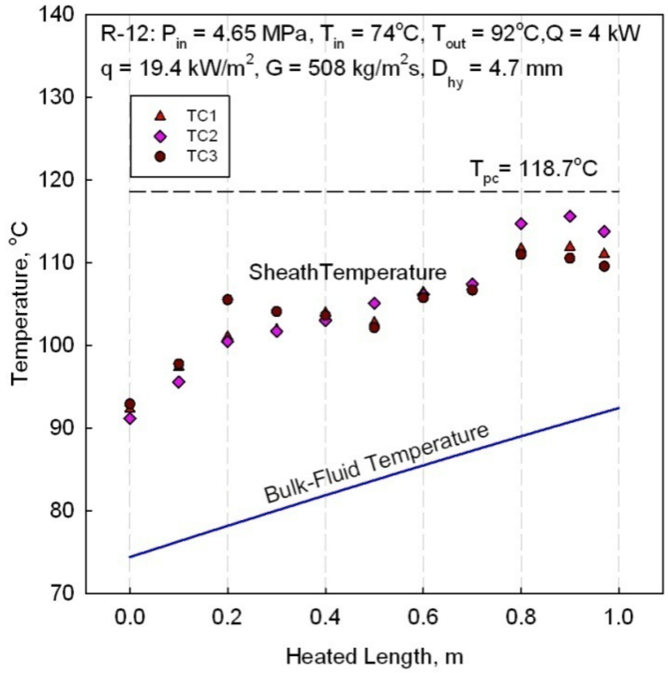

Figure 5: Central Sheath and Bulk-Fluid Temperature Profiles of Experiment 1.

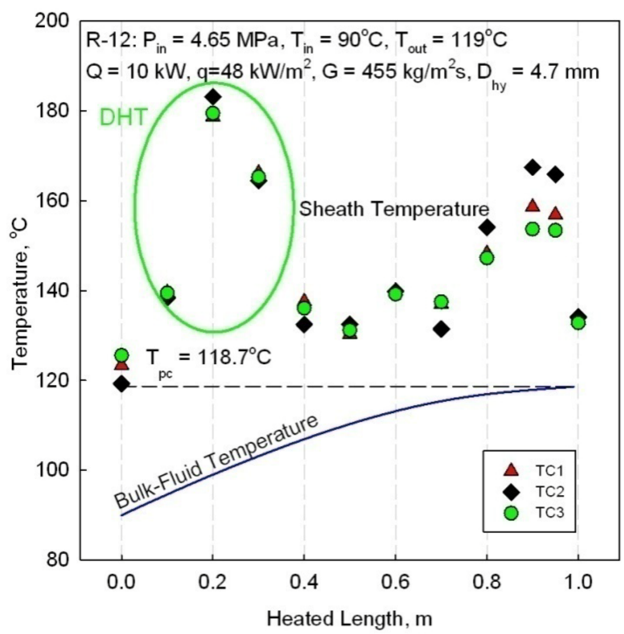

Figure 6: Results of Experiment 2.

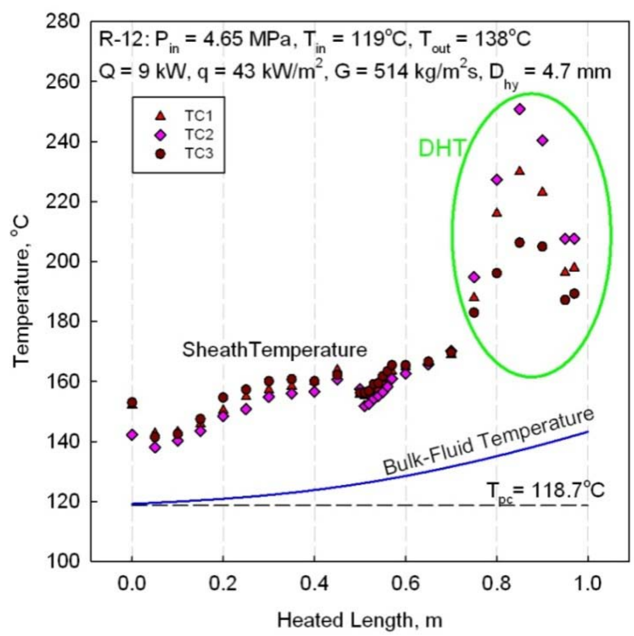

Figure 7: Results of Experiment 3.

Figure 7 depicts the experimentally measured sheath temperature and calculated temperature profile of the coolant corresponding to Experiment 3. The inlet temperature of the coolant was slightly above the pseudocritical temperature of 118.7℃ and rose approximately to 140℃. A region of DHT was observed towards the outlet of the channel resulting in a significant rise in the sheath temperature as indicated by the green oval. Reference [8] identifies $q/G \geq 0.07 - 0.1$ (kJ/kg) as the onset of DHT. This ratio was 0.04, 0.11, and 0.08 for Experiments 1, 2 and 3, respectively, which indicates that a DHT regime was theoretically expected for Experiments 2 and 3. However, there is no correlation available to calculate the HTC in a DHT regime.

5.4 Comparison of Correlations with Experimental Data

The HTC and sheath temperature profiles were calculated based on the Bishop et al., Mokry et al., Swenson et al., and Gorban et al. correlations. The results are shown in Figs. 8, 9, and 10. As shown in Fig. 8, the HTC and sheath temperature of Experiment 1 were best predicted by the Swenson et al. correlation. Figure 9 depicts the HTC and sheath temperature of Experiment 2 along the heated length of the test section. These correlations predicted neither the DHT regime in the entrance region, nor the reduction in the HTC towards the outlet of the channel. However, the HTC calculated using the Mokry et al. correlation best fit the experimental data and provided a conservative solution.

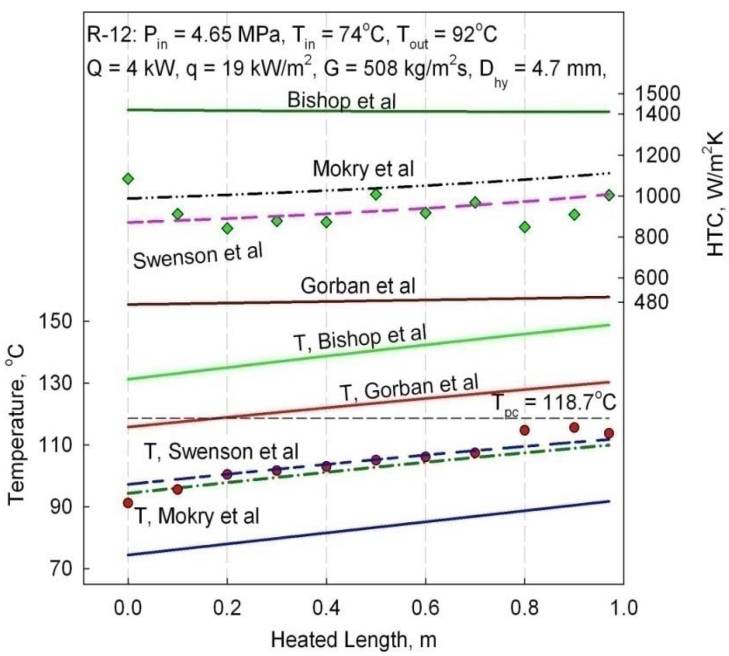

Figure 8: Calculated and Experimental HTC and Central Sheath Temperature Profiles of Experiment 1.

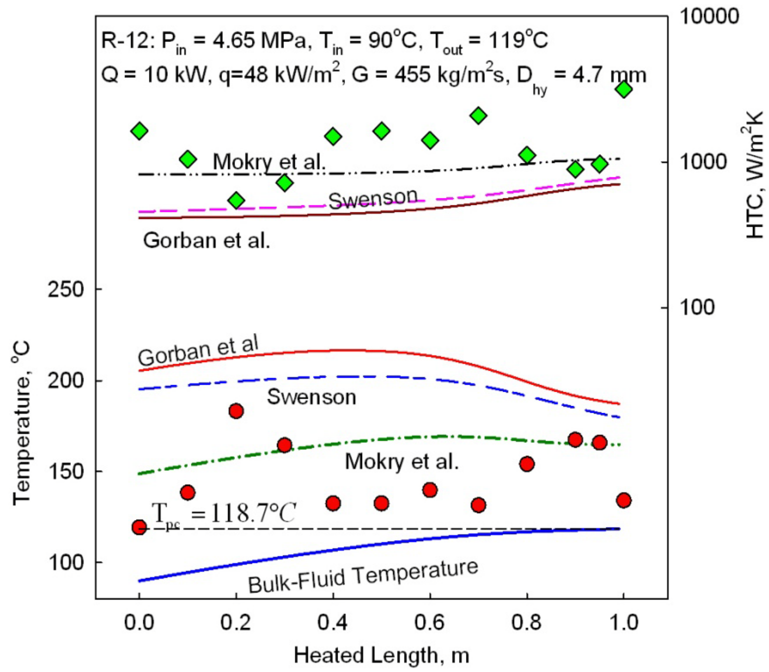

Figure 9: Calculated and Experimental HTC and Central Sheath Temperature Profiles of Experiment 2.

Figure 10 shows the HTC and sheath temperature of Experiment 3. The increase in HTC in the beginning of the channel due to the entrance effect was not predicted with any of the examined correlations. None of these correlations predicted the DHT regime observed towards the outlet of the test section.

Heat transfer can become deteriorated for certain relationships between the heat flux and the mass flux which leads to an increase in the surface temperature of the sheath. Richards et al. [8] identifies the ratio $q/G > 0.07$— 0.1 kJ/kg as the onset of DHT regime for Freon-12. Additionally, for water flowing in a round smooth tube, the onset of DHT is identified as $q/G >$ 0.8 kJ/kg [9].

The mass flux and heat flux of the proposed CANDU-SCWR are 1172 kg/m²· s and 970 kW/m² [10], respectively, based on a Variant-20 fuel bundle. The q/G ratio for the CANDU-SCWR is approximately 0.82 kJ/kg which indicates that a DHT regime is expected. However, in the CANDU-SCWR fuel-channel the flow is considered to be turbulent form the inlet of the fuel-channel; therefore, the onset of the DHT regime may be higher than 0.8 kJ/kg. This does not eliminate the possibility of occurrence of a DHT regime, which would in turn increase the sheath temperature. Additionally, a DHT regime would result in a drop in the HTC, which in turn would increase the fuel centreline temperature significantly. Since fuel matrix and sheath are considered as the first two barriers against the release of fission products, it is necessary to perform the design based on a correlation that predicts the DHT.

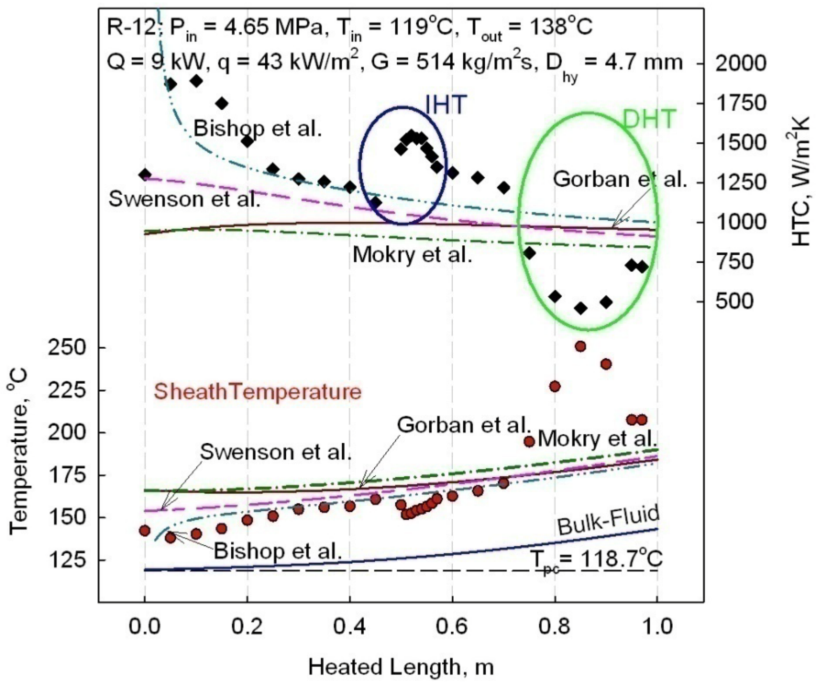

Figure 10: Calculated and Experimental HTC and Central Sheath Temperature Profiles of Experiment 3.

6. Conclusion

Three experiments have been conducted in a 7-element bundle inside a hexagonal flow channel when Freon-12 was used as a coolant with downward vertical flow through the test section. Under some combination of heat flux and mass flux, deteriorated heat transfer regime was observed. Bulk-fluid and central sheath temperature profiles were calculated using various correlations. The results of analysis showed that available correlations do not predict the deteriorated heat transfer regime. A correlation, which predicts the DHT regime, is needed for developing a sub-channel code for SCWRs.

ACKNOWLEDGEMENTS

Financial supports from the NSERC/NRCan/AECL Generation IV Energy Technologies Program and NSERC Discovery Grant are gratefully acknowledged.

REFERENCES

[1] Pioro, I. L., & Duffey, R. (2007). *Heat Transfer and Hydraulic Resistance at Supercritical Pressure in Power-Engineering Applications.* New York, USA: ASME Press.

[2] Bae, Y.-Y., & Kim, H.-Y. (2009). Convective heat transfer to CO_2 at a supercritical pressure flowing vertically upward in tubes and an annular channel. *Experimental Thermal and Fluid Science* , Vol. 33, No. 2, pp. 329-339.

[3] Grabezhnaya, V. A., & Kirillov, P. L. (2006). Heat Transfer at Supercritical Pressuresand Heat Transfer Deterioration Boundaries. *Thermal Engineering* , Vol. 53, No. 4, pp. 296–301.

[4] EPA. (2009, September 3). *Guidance on Retrofitting to HFC-134a*. Retrieved March 18, 2010, from United States Environmental Protection Agency: http://www.epa.gov/ozone/title6/609/technicians/retrguid.html

[5] NIST Reference Fluid Thermodynamic and Transport Properties—REFPROP, 2007. NIST Standard Reference Database 23, Ver. 7.0, E.W. Lemmon, M.O. McLinden and M.L. Huber, National Institute of Standards and Technology, Boulder, CO, U.S. Department of Commerce, April.

[6] Mokry, S., Gospodinov, Y., Pioro, I., & Kirillov, P. (2009). Supercritical Water Heat-Transfer Correlation for Vertical Bare Tubes. *ICONE-17.* Brussels: ASME.

[7] Incropera, F. P., Dewitt, D. P., Bergman, T. L., & Lavine, A. S. (2006). Fundamentals of Heat and Mass Transfer. John Wiley & Sons.

[8] Richards, G., Milner, A., Pascoe, C., Patel, H., Peiman, W., Saltanov, E., et al. (2010). Heat Transfer in a Vertical 7-Element Bundle Cooled with Supercritical Freon-12. *The 2nd Canada-China Joint Workshop on Supercritical Water-Cooled Reactors.* Toronto, Canada: CNS.

[9] Grabezhnaya, V. A., & Kirillov, P. L. (2006). Heat Transfer under Supercritical Pressures and Heat Transfer Deterioration Boundaries. *Thermal Engineering, Vol. 53, No. 4,* , 296–301.

[10] Naidin, M., Mokry, S., & Pioro, I. (2009). SCW NPPs: Layouts and Thermodynamic Cycles. *International Conference Nuclear Energy for New Europe* . Bled, Slovenia.